*Technology and Science for the Ships of the Future*
*V. Crupi and V. Bucci (Eds.)*


*doi:10.3233/PMST250099*

# Numerical Simulations of a Bulk Carrier with Flettner Rotors Using a Fully Nonlinear Potential Flow Solver

Manuel COPPOLA [a,1], Francesco COSLOVICH [b], Mitja MORGUT [a]
[a] *University of Trieste, Department of Engineering and Architecture, Trieste, Italy*
[b] *FLOWTECH International AB, Gothenburg, Sweden*

**Abstract.** In order to tackle emissions reduction and the decarbonization of the maritime industry, increasing effort is put into finding other means to propel a ship. In this respect, wind-assisted propulsion is becoming increasingly popular, with Flettner rotors being one of the preferred choices thanks to their simplicity and the possibility of retrofitting existing vessels. To obtain reliable predictions of the fuel-saving capabilities coming from the use of the rotors, it is important to carry out numerical simulations considering realistic scenarios. For this aim, in this paper, a fully nonlinear unsteady potential flow method is employed to simulate free sailing conditions. Ad-hoc simplified models are implemented to mimic propeller and rudder actions. To address viscous effects affecting free sailing, virtual captive tests have been performed with a viscous solver and the manoeuvring coefficients are added to the equations of motion of the potential flow method. A simplified model for the wind and for Flettner rotors is also included in the solver. Results from simulations of a bulk carrier in calm water under different wind conditions are presented.

**Keywords.** Flettner Rotors, BEM, Numerical Simulation, Seakeeping, Manoeuvring

## 1. Introduction

Maritime transport is essential for global trade, carrying about 90% of goods worldwide. However, it also has a significant environmental impact due to emissions of greenhouse gases (GHG), sulfur oxides ($SO_x$) and nitrogen oxides ($NO_x$). To mitigate these effects, the International Maritime Organization (IMO) has introduced regulations such as the Energy Efficiency Design Index (EEDI) and MARPOL Annex VI, imposing stricter limits on fuel consumption and emissions. While these measures have driven improvements, the industry still faces challenges in meeting long-term decarbonization goals. As a result, there is growing interest in alternative propulsion technologies to further enhance energy efficiency and reduce emissions.

One promising solution is Wind-Assisted Ship Propulsion (WASP), which utilizes wind thrust to assist conventional engines and lower fuel consumption. Various WASP

[1]Corresponding Author: Manuel Coppola, University of Trieste, Department of Engineering and Architecture, Trieste, Italy; E-mail: manuel.coppola@studenti.units.it

technologies have been tested, including rigid sails, suction wings, kite-assisted propulsion and Flettner rotors, as presented in [1]. Recognizing their potential, the IMO has incorporated WASP into its decarbonization strategies, as noted in [2].

To predict and optimize the effects of WASP systems, computational methods are often used. Reynolds-Averaged Navier-Stokes Equations (RANSE) solvers provide detailed simulations of flow around a ship, including viscosity effects, but require substantial computational resources. In contrast, potential flow methods are faster and more often used during initial design stages, though they neglect viscosity and are less accurate in capturing complex interactions between the hull and the surrounding flow. To overcome these limitations, hybrid approaches combine both methods, achieving a balance between accuracy and efficiency.

In this study, numerical simulations using *Shipflow MOTIONS*, a fully nonlinear unsteady potential flow method, have been carried out to predict the performance of a free-sailing ship with Flettner rotors. The viscous forces typical of a manoeuvring problem have been evaluated performing Virtual Captive Tests (VCT) using the RANSE solver of *Shipflow* and added to the equation of motions of the potential flow solver. The numerical results were then compared with experimental data presented in [3].

## 2. Mathematical Model and Numerical Approach

A description of the mathematical and numerical models will be given in this section. For a more detailed description of the method see [4]. Assuming the fluid is homogeneous, inviscid, incompressible and irrotational, the velocity field can be represented by a scalar quantity $\phi$, called velocity potential, that satisfies Laplace's equation:

$$\nabla^2 \phi = 0 \tag{1}$$

To solve the Boundary Value Problem (BVP) defined in this way, boundary conditions have to be introduced on the domain. On the free surface, the kinematic and dynamic boundary conditions must be applied. The kinematic condition is given by:

$$\frac{D\mathbf{x}}{Dt} = \nabla \phi \tag{2}$$

where $\mathbf{x} = (x, y, z)$ represents the position of a fluid particle on the free surface and $\frac{D*}{Dt}$ denotes the material derivative, defined as:

$$\frac{D*}{Dt} = \frac{\partial *}{\partial t} + \nabla \phi \cdot \nabla * \tag{3}$$

The dynamic condition is defined as:

$$\frac{D\phi}{Dt} = -gz + \frac{1}{2} \nabla \phi \cdot \nabla \phi - \frac{p_a}{\rho} \tag{4}$$

where $g$ is the gravitational acceleration, $\rho$ is the fluid density and $p_a$ is the atmospheric pressure. The impermeability condition is imposed on the instantaneous wetted hull and on the bottom of the domain. It is defined as:

$$\nabla\phi \cdot \mathbf{n} = \begin{cases} \mathbf{n} \cdot (\mathbf{u} + \omega \times \mathbf{r}) & \text{on the body surface} \\ 0 & \text{on the bottom} \end{cases} \tag{5}$$

where $\mathbf{n}$ is the normal to the surface, $\mathbf{u} = (u, v, w)$ and $\omega = (p, q, r)$ are the translational and angular velocity vectors, respectively, and $\mathbf{r}$ is the distance between the surface and the center of rotation.

The BVP is solved using a Boundary Element Method (BEM), where the domain is discretized using quadrilateral panels, each with an unknown source distribution of constant strength. The evolution in time of the free surface is obtained with a Mixed Eulerian-Lagrangian (MEL) approach, as described in [5], using the Adams-Bashforth-Moulton method for the integration in time.

To prevent wave reflections at domain boundaries, a damping zone is introduced, ensuring the solution from the inner and outer domains matches at the intersection. The damping zone phases out the scattered part of the solution due to the presence of the hull.

Once the source strength distribution has been determined at each point of the domain after solving the BVP, the velocity potential and the velocity on each panel can be evaluated. The pressure can then be obtained on the wetted hull using the unsteady Bernoulli's equation, defined as:

$$p = -\rho \left( \frac{\partial \phi}{\partial t} + \frac{1}{2} |\nabla \phi|^2 + gz \right) \tag{6}$$

composed respectively of the partial time derivative of the velocity potential, the kinetic energy and the hydrostatic energy components. By integrating the pressure over the wetted hull surface, the hydrodynamic forces and moments acting on the body can be obtained to solve the ship motion equations. These quantities are formulated as:

$$\mathbf{F} = -\iint_{S_b} p\mathbf{n}\, dS + \mathbf{F_{ext}} \tag{7}$$

$$\mathbf{M} = -\iint_{S_b} p(\mathbf{r} \times \mathbf{n})\, dS + \mathbf{M_{ext}} \tag{8}$$

where $\mathbf{F} = (F_1, F_2, F_3)$ represents the vector of forces, $\mathbf{M} = (M_1, M_2, M_3)$ the vector of moments and $S_b$ the wetted hull surface. Since the method is based on potential flow, integrating the pressure yields only inviscid forces and moments. External forces $\mathbf{F_{ext}}$ and $\mathbf{M_{ext}}$ can be added to the equation of motions to include effects which are not accounted for by the potential flow solver.

External forces include for example viscous drag, forces from the VCT, forces from the propeller and forces from the Flettner rotors. Viscous forces typical of the manoeuvring problem are estimated by means of VCT: the viscous solver is used to obtain the forces acting on the hull at different drift angles, turning circle radii and a combination of the two. Through a least square method fitting, surge and sway forces as well as yaw moment are expressed as a function of sway and yaw velocities. A comparison between numerical simulations using the same solver and methodology and experimental results was presented in [6], showing good agreement. The manoeuvring coefficients obtained in this way are added into the equation of motions to take into account viscous forces which cannot be obtained with the potential flow solver. Rudder, propeller, engine, wind, and

rotor effects are modeled using simplified approaches. The rudder model considers flow interaction effects, including propeller slipstream, hull-induced flow straightening and nonlinear lift and drag behaviors across stall regimes. A PID controller is implemented to keep the course or the heading if needed. The propeller model uses open water curves to obtain the thrust and the torque. The advanced velocity is evaluated at the propeller disk position taking into account local velocities and the wake obtained from viscous calculation. Once the advance ratio is calculated with these velocities, thrust and torque coefficients are extracted from the open water curves. For a more detailed description of the models used, see [7].

The wind model follows a power-law profile to account for velocity variation along the vertical axis:

$$U_w(z) = U_{ref}\left(\frac{z}{z_{ref}}\right)^{\frac{1}{\sigma}} \tag{9}$$

with $\sigma = 9$ being the inverse Bellman coefficient over open water and $z_{ref}$ the reference height. Flettner rotors are discretized into horizontal strips, each contributing to lift and drag forces, with total aerodynamic loads obtained by superposition. The spin ratio ($SR$) characterizes rotor operation. Lift and drag coefficients ($C_L, C_D$) are obtained from CFD-based regression analyses and are functions of $SR$, aspect ratio $AR = d/H$ and normalized end-plate diameter ($d_e/d$). For a more detailed description of the wind and rotor models, see [3].

## 3. Numerical Setup

The present study investigates the free-sailing behavior of a vessel equipped with four Flettner rotors, evenly spaced on the deck of the ship, analyzing its response under different wind conditions in calm water. The objective is to assess the efficiency of the Flettner rotors and compare the results with the experiments presented in [3]. The hull tested is the *SINTEF Ocean Bulk Carrier SOBC-1* presented in [8].

The computations performed with Flettner rotors have the ship in a free sailing configuration. The propulsion is achieved using the models described in the previous section for the propeller and the delivered power. To closely replicate the experiment, the experimental values of wake, thrust deduction factor, open water characteristics of the propeller, and the form factor presented in [8] are used. The engine-propeller system is set up to ensure a speed of the ship of 12.25 kn with constant rps.

All the numerical simulations are performed in calm water considering true wind angles of 60°, 90°, 120°, and 150°, with wind speeds of 10 m/s and 20 m/s. The wind profile follows a power-law formulation with a reference height $z_{ref}$=20 as described in the previous section.

The Flettner rotors are discretized into 11 horizontal strips. It is important to point out the limitations of the model adopted regarding the range of validity of the $SR$: $SR \in [1,3]$. When the values exceed the range of validity, the closest value was selected. In order to replicate the experiments, the interaction between the rotors is not considered.

The computational domain is discretized using a fixed grid for the hull and an adaptive grid refinement technique for the free surface, updated at each time step. In both

cases, a fine grid is used to discretize the domain. The hull is discretized with 8800 panels. The free surface accounts for approximately 2400 panels at the beginning and 9000 after the flow has stabilized.

## 4. Results

In this section, the numerical results are presented and compared with the experimental results available.

In Fig. 1 the key parameters showing the effects of the rotors on the hull are presented. As can be seen, there is generally good agreement between simulations and experiments. The heel and trim angles are well captured by the solver, showing that the hydrodynamic forces are solved accurately. Furthermore, the speed is very similar to the experimental values, showing the beneficial effects of the rotor sails, particularly within the True Wind Direction (TWD) range of 60° to 150°, with the maximum effect occurring under beam wind conditions. The performance gains shown by the increase of speed are associated with the thrust contribution provided by the rotor sails. In configurations where the speed increase is more pronounced, the rotor thrust constitutes a significant portion of the total propulsion. Specifically, under beam wind conditions, the rotor thrust accounted for up to 35% of the total thrust at 10 m/s and up to approximately 80% at 20 m/s. For higher wind speeds the results appear to be slightly overestimated, although the general trend remains consistent.

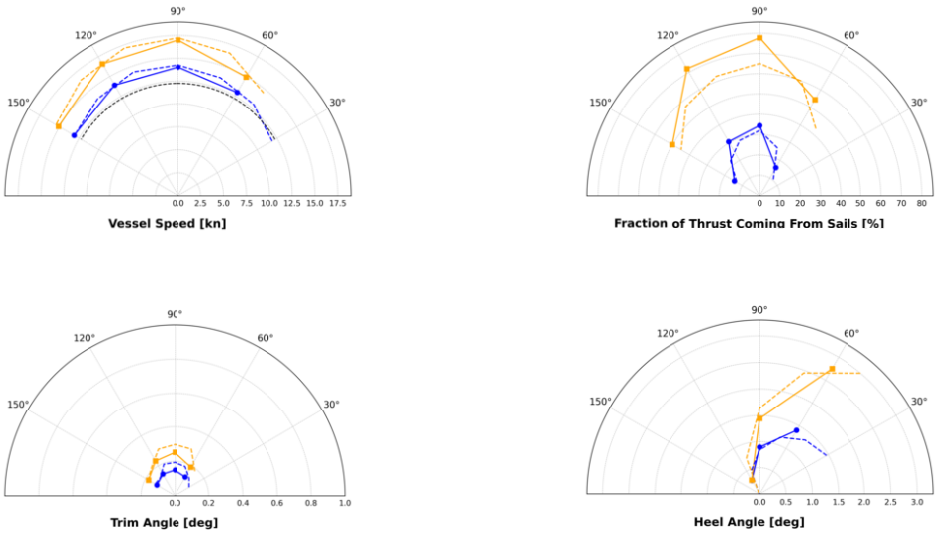


**Figure 1.** Comparison of parameters describing the effect of rotors on the hull: numerical results (solid lines) and experimental data (dashed lines) at 10 m/s (blue) and 20 m/s (orange). The dashed black line represents the case without rotors at 12.25 knots.

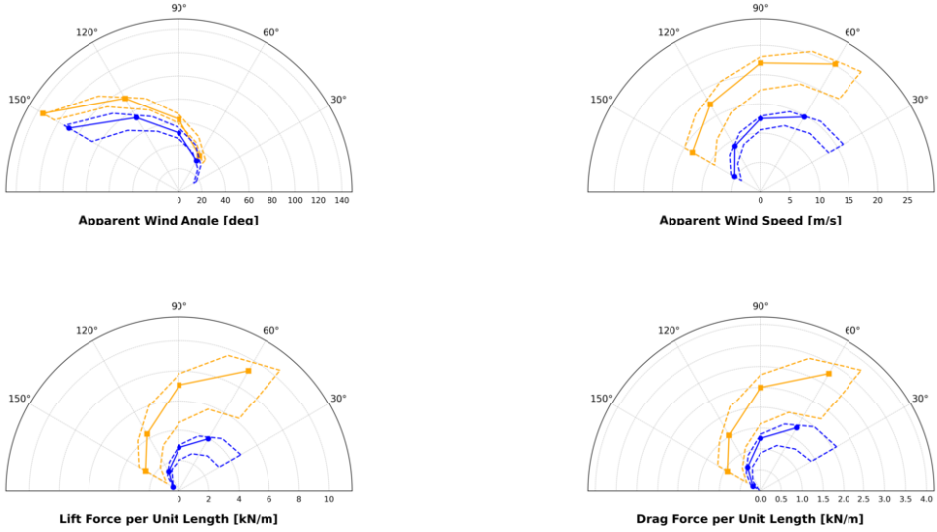


**Figure 2.** Comparison of parameters describing the aerodynamic behavior of the rotors: numerical results (solid lines) and experimental data (dashed lines) at 10 m/s (blue) and 20 m/s (orange).

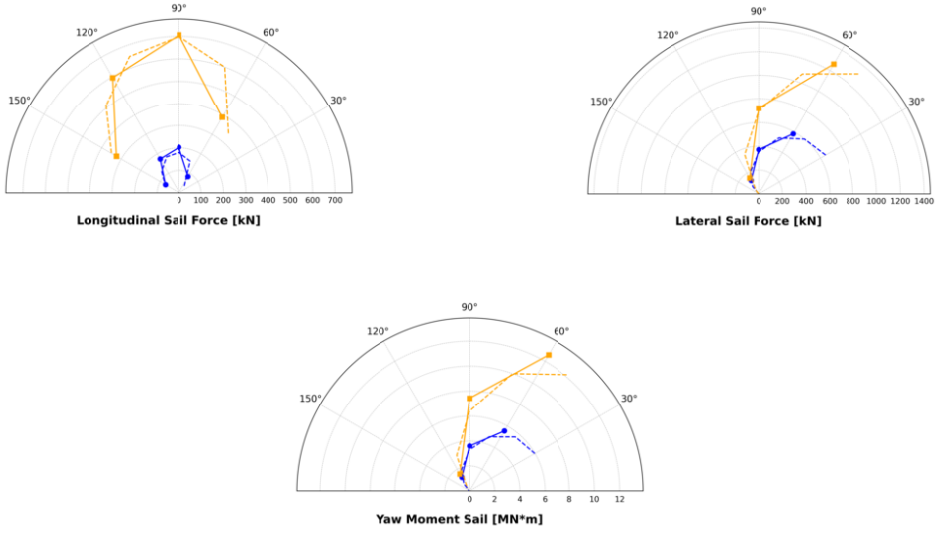


**Figure 3.** Comparison of parameters describing the forces and moments generated by the rotors on the hull: numerical results (solid lines) and experimental data (dashed lines) at 10 m/s (blue) and 20 m/s (orange).

Fig. 2 shows the aerodynamic parameters of the rotors. Experimental data are displayed as a range of values, while numerical results are shown as single values. The experimental results plot the maximum and minimum values for each Flettner rotor, while the results from the numerical simulations show the corresponding value at the center of effort of the rotor. Apparent wind, lift, and drag are computed taking into account the dynamics of the ship at each time step. As can be seen, the computed values show good agreement with the experimental model.

In Fig. 3 the forces and the yaw moment generated by the rotors acting on the ship are shown. A good agreement between numerical simulations and experimental data can be seen for these quantities too. As expected, the maximum longitudinal force is generated for TWD between 90° and 120°.

## 5. Conclusions

In this study, a hybrid approach was adopted to predict and analyze the effect of Flettner rotors on ship performance, using the *SINTEF Ocean Bulk Carrier SOBC-1* as a case study. This approach uses a fully nonlinear unsteady potential flow method to simulate the performance of a free-sailing ship. The viscous manoeuvring forces were evaluated by performing Virtual Captive Tests on the hull and extracting the manoeuvring coefficients. These coefficients were then added to the equations of motion of the potential flow solver.

Simulations were performed in calm water conditions and under different true wind angles. The results were then compared with experimental data available in the literature [3]. The numerical results show good agreement with experimental data, accurately capturing the aerodynamic behavior and the overall impact of rotor sails on vessel performance, while remaining within the applicability limits of the rotor sails model. The simulations confirm that Flettner rotors provide the most beneficial effects in the range between 90° and 120°.

These results underscore the main advantage of the proposed methodology: the ability to perform both maneuvering and free-sailing simulations while incorporating external wind-assisted propulsion models. Further investigations could focus on the effect of Flettner rotors under combined wind and wave conditions, also taking into account the mutual interaction between the cylinders in order to represent more realistic scenarios.

## 6. Acknowledgements

The authors wish to thank the research institute SINTEF Ocean, Norway, for sharing the experimental dataset of the *SINTEF Ocean Bulk Carrier SOBC-1*, presented in [8], which served as a valuable benchmark for validating the numerical results obtained in this work.

## References

[1] Khan L, Macklin J, Peck B, Morton O, Souppez J-B. A review of wind-assisted ship propulsion for sustainable commercial shipping: latest developments and future stakes. Wind Propulsion 2021, doi: 10.3940/rina.win.2021.05

[2] International Maritime Organization (IMO). Fourth IMO Greenhouse Gas Study 2020, London, 2020.
[3] Sauder T, Alterskjær SA. Hydrodynamic testing of wind-assisted cargo ships using a cyber–physical method. Ocean Engineering 2022; 243:110206, doi: 10.1016/j.oceaneng.2021.110206
[4] Coslovich F, Kjellberg M, Östberg M, Janson CE. Added resistance, heave and pitch for the KVLCC2 tanker using a fully nonlinear unsteady potential flow boundary element method. Ocean Engineering 2021; 229:108935, doi: 10.1016/j.oceaneng.2021.108935
[5] Longuet-Higgins MS, Cokelet ED. The deformation of steep surface waves on water – I. A numerical method of computation. Proceedings of the Royal Society A: Mathematical, Physical and Engineering Sciences, 1976.
[6] Alexandersson M., Korkmaz K.B., Mazza G.: Virtual Captive Tests with a destroyer hull form. Numerical Towing Tank Symposium, 2017.
[7] Kjellberg M, Gerhardt F, Werner S. Sailing performance of wind-powered cargo vessel in unsteady conditions. Journal of Sailing Technology 2023; 8:218–254, doi: 10.5957/jst/2023.8.12.218
[8] Krasilnikov, V.I. (2022): SINTEF Ocean Benchmark Bulk Carrier SOBC-1, Presentation at the 1$^{st}$ Meeting of the International Collaboration Network in Marine Technology, Trondheim, Norway, May 03, 2022 (virtual event).